[Original paper]
Journal of the Korean Society for Nondestructive Testing
Vol. 32, No. 2 (2012. 4)

A Brief Overview of a Scale Independent Deformation Theory and Application to Diagnosis of Deformational Status of Solid-State Materials

Sanichiro Yoshida

Abstract A field theoretical approach to deformation and fracture of solid-state material is outlined, and its application to diagnosis of deformational status of metal specimens is discussed. Being based on a fundamental physical principle known as local symmetry, this approach is intrinsically scale independent, and capable of describing all stages of deformation on the same theoretical foundation. This capability enables us to derive criteria that can be used to diagnose transitions from the elastic to plastic regime, and the plastic to fracturing regime. For practical applications of these criteria, an optical interferometric technique known as electronic speckle-pattern interferometry is proved to be quite powerful; it is able to visualize the criteria as a whole image of the object on a real-time basis without numerical processing. It is demonstrated that this method is able to reveal loading hysteresis as well.

Keywords: Plastic Deformation, Fracture, Load Hysteresis, Electronic Speckle-Pattern Interferometry

1. Introduction

Structures and machines often fail after they pass periodic inspections, leading to catastrophic accidents. In particular, failures of aircrafts in normal flight shortly after they pass the pre-flight inspections are of extremely tragedy. They must be prevented. Currently prevailing inspection technologies mostly focus on the detection of cracks at the earliest stage as possible. Recent advancements in the related field such as ultrasonic technology allow inspectors to detect micro-cracks at an early stage. However, it is unclear whether the accidents occur due to micro-cracks overlooked during the inspection, or due to micro-cracks newly generated after the inspection.

These problems arise partly from limitations of the theory that the inspection procedure is based on. The limitation of the current theory for accurate fracture prediction is mostly due to the lack of a solid physical foundation on which the stages before and after micro-cracks appear are connected. Conventional fracture mechanics [1] is successful for a number of applications, but it basically describes how a crack develops from its initial stage, and relies on elastic theory to formulate the fracturing process. If we can predict crack generation at an earlier stage, inspection technology will drastically advance, and the number of catastrophic accidents will be decreased. Development of inspection techniques based on a theory capable of describing deformation and fracture on the same theoretical foundation is essential.

In this respect, the field theoretical approach to deformation and fracture that the author has been studying for the last 20 years has great advantage[2-4]. The theoretical foundation of this approach is originally developed by Panin

[Received: February 27, 2012, Revised: April 10, 2012, Accepted: April 13, 2012] Department of Chemistry and Physics, Southeastern Louisiana University, SLU 10878, Hammond, LA 70402, USA (E-mail: syoshida@selu.edu)

et al.[5,6]. Being based on a fundamental principle of physics known as local (gauge) symmetry[7], the theory is capable of describing deformation dynamics of all stages without relying on phenomenology; hence by nature, it is scale independent. It postulates that we can always find a local region where the deformation can be expressed by the formalism of conventional linear elasticity[8], and nonlinear dynamics in the plastic regime can be formulated as the interaction among those local dynamics. This interaction holds the entire object to be one continuum. When the global dynamics associated with this interaction stops operating, the material fractures.

This field theoretical approach derives plastic deformation and fracture criteria[9] that are fundamentally different from conventional approaches. Past experiments[10] support the validity of these criteria under certain conditions. For practical applications of this approach, an optical interferometric technique known as the electronic speckle-pattern interferometry(ESPI) [11] is quite useful. It can visualize the criteria as a whole image of interferometric fringe pattern on a real-time basis.

The aim of this paper is to briefly outline the gist of the field theoretical approach and to discuss supporting ESPI experiments. One of the experiments demonstrates that the present plastic deformation and fracture criteria can be used to diagnose load hysteresis of metal specimen.

2. Theoretical Overview

2.1 Field Equation

Details about the present field theory can be found elsewhere[2-5]. In short, its gist can be described as follows. In conventional continuum mechanics[12,13], deformation is described as an orientation preserving transformation (mapping) ϕ of points on the material[12]. Usually, the initial (before the deformation) points are expressed in the Lagrangian coordinates affixed to the material, and the final (after the deformation) points are expressed in the Eulerian coordinates. The deformation is expressed by the deformation gradient tensor of the following form.

$$F_{ij} = \frac{\partial \phi^i}{\partial x^j} \tag{1}$$

Here ϕ^i is the *i-th* component in the final (Eulerian) coordinates and x^j is the *j-th* component in the initial (Lagrangian) coordinates. Note that eqn. (1) is expressed by the common differential operation. Note that we can use the same differential operation because the mathematical expressions of the "before" and "after" deformation are connected via the orientation preserving mapping ϕ.

Being an orientation preserving transformation, the mapping basically describes stretch and compression of the material, as each of ϕ in Fig. 1 illustrates schematically. This is why we can always find the principal coordinates system in which the strain and stress matrices have only normal components, not a shear component. This formalism is therefore inapplicable to the plastic regime where the deformation is nonlinear and cannot be expressed without shear components.

The present field theory solves this problem as follows. The theory postulates[4] that in the plastic regime the deformation can still be described as linear elasticity if the volume of analysis is sufficiently small. This postulate can be justified by the fact that it is always possible

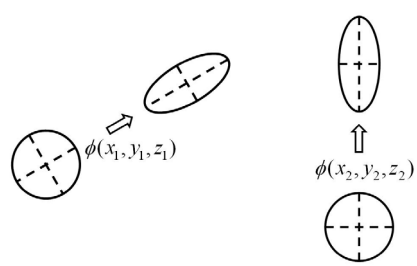

Fig. 1 Conceptual figure of mapping

to find a local region where the inter-atomic potential can be approximated by a quadratic function of the inter-atomic distance. As an example, Lenard-Jones potential is quadratic near the equilibrium. Then the field theory postulates that in the plastic regime the material experiences a number of local linear elastic deformations where each of them can be expressed by the locally defined orientation-preserving mapping, as Fig. 1 illustrates schematically.

This treatment brings some complexity regarding the operation of differentiation. Now that each local region has its own preserved orientation, the differentiation cannot be defined globally. In other words, if we displace from one global coordinate point to another, we know that the orientations associated with the local mapping of the first point and the second point are different. Consequently, if we find a difference in deformation, i.e., different values in the deformation gradient tensor between the two local deformations, it is not clear if the difference comes from the actual difference in deformation (physics) or from the difference in the local preserved orientations (geometry). To describe the deformation in the global coordinates, it becomes necessary to separate the change due to the physics and to the geometrical difference. The present field theory handles this problem by isolating the rotational part of kinematics from the formalism representing the deformation; more specifically, by viewing rotation as coordinate dependent potential not part of the deformation[4]. The local region that obeys linear elasticity is called the deformation structural element[2,6].

In this way, the entire formulation is divided into two portions; the first portion is to represent the deformation using the same formalism as the local linear elasticity in respective deformation structural elements, and the second portion is to represent rotation of structural deformation elements via the potential. Thus the law of elasticity is conserved, and at the same time, the nonlinearity is taken into consideration. The potential can be viewed as representing interaction among deformation structural elements. Naturally, when the entire material experiences linear elastic deformation, the potential becomes null. The situation is similar to general relativity and special relativity. When the space-time is curved, although special relativistic formalism hold locally, it is necessary to consider interaction among local frames, and the gravitational potential governs the interaction [14].

The equations that govern the nonlinear dynamics can be derived through application of the least action principle to this potential[7]. After some mathematical procedures, the following governing equations can be derived [3-5]. Since these equations describe the field associated with the potential, they are called the field equations.

$$\nabla \cdot \vec{v} = j^o \tag{2}$$

$$\nabla \times \vec{v} = \frac{\partial \vec{\omega}}{\partial t} \tag{3}$$

$$\nabla \times \vec{\omega} = -\frac{1}{c^2}\frac{\partial \vec{v}}{\partial t} - \vec{j} \tag{4}$$

$$\nabla \cdot \vec{\omega} = 0 \tag{5}$$

where $\vec{\nu}$ is the velocity, $\vec{\omega}$ is rotation of the material points and related to $\vec{\nu}$ by eqn. (3), and c is the phase velocity of the wave characteristics of the displacement field. j^o and $\vec{j}$ are known as the current of symmetry[7]. Explanations of the currents are given elsewhere [3,7]

The physical meaning of each equation can be given as follows. The left-hand side of eqn. (2) represents the net flow of particles into a local region. j^o on the right-hand side represents the rate of material flowing out the unit volume.

If the mass of the local volume is multiplied, eqn. (2) represents the net momentum change. Eqn. (3) defines the rotation associated with the potential. Eqn. (4) represents the interaction between the translational and rotational mode of displacement. This is the most important equation from the viewpoint of dynamics in the plastic regime, and will be discussed in the next section. The last equation indicates that the dynamics associated with the rotation does not have a source. Instead, the rotational field exerts force via $\nabla\times\vec{\omega}$ in eqn. (4), as explained in more detail below.

2.2 Plastic Deformation Dynamics

To explore the physical meaning of eqn. (4), let's rearrange the terms as follows[2,4].

$$\frac{1}{c^2}\frac{\partial\vec{v}}{\partial t}=-\nabla\times\vec{\omega}-\vec{j} \tag{6}$$

Since c represents the phase velocity of a displacement wave, its square has a general form of density/stiffness. More detailed analysis [15] indicates that if we put the phase velocity as

$$c^2=\frac{\mu}{\rho} \tag{7}$$

and $\vec{j}$ as

$$\vec{j}=-\frac{\lambda+2\mu}{\mu}\nabla(\nabla\cdot\vec{\xi}) \tag{8}$$

eqn. (6) reduces to Cauchy's equation of motion as below.

$$\rho\frac{\partial^2\vec{\xi}}{\partial t^2}=\mu\nabla^2\vec{\xi}+(\lambda+\mu)\nabla(\nabla\cdot\vec{\xi}) \tag{9}$$

Here ρ is the density of the material, and λ and μ are the first and second Lamé's constant.

Eqn. (8) represents the net longitudinal force exerted by the neighboring volumes on the unit volume as the differential elastic force at the boundaries. Note that in the elastic case, the right-hand side of eqn. (6) has only longitudinal components. This is because linear elasticity is essentially an orientation preserving transformation as discussed above. This is evidenced by the fact that we can always find a principal coordinate system in which the stress and strain tensors have only normal components, not a shear component.

In the plastic regime, basically two changes happen. First, $\vec{j}$ does not represent longitudinal elastic force. Instead, it represents momentum flow out of the unit volume. To understand this let's apply the divergence to both-hand sides of eqn. (6). Using the identity $\nabla\cdot(\nabla\times\vec{\omega})=0$ and eqn. (7) we obtain the following equation.

$$\mu(\nabla\cdot\vec{j})=-\frac{\partial(\nabla\cdot\rho\vec{v})}{\partial t} \tag{10}$$

Eqn. (10) is the so-called equation of continuity. From the form of this equation, $\mu\vec{j}$ can be identified as the flow of $(\nabla\cdot\rho\vec{j})$ that compensates the temporal change of $(\nabla\cdot\rho\vec{v})$ represented by the right-hand side. Since $(\nabla\cdot\rho\vec{v})$ is the divergence of the momentum from the unit volume, $\mu\vec{j}$ can be identified as the temporal change in the differential momentum, which is basically the net external force (Newton's second law). More detailed analysis [15] indicates that in this situation $\mu\vec{j}$ can be put in the following form.

$$\mu\vec{j}=-(\nabla\cdot\rho\vec{v})c\hat{k} \tag{11}$$

Here $\hat{k}$ is the unit vector in the direction of the displacement wave propagating at the phase velocity c [eqn. (7)]. With the longitudinal effect not representing force, it does not have contribution to the wave dynamics.

Consequently, in the plastic regime the displacement wave is transverse. With eqn. (11), the equation of motion in the plastic regime can be put as follows.

$$\rho\frac{\partial\vec{v}}{\partial t}=-\mu\nabla\times\vec{\omega}-\rho c(\nabla\cdot\vec{\xi})\hat{k} \tag{12}$$

The second change in transition from the elastic to plastic regime is that the stress field starts to have shear components even expressed in the principal coordinate system. In other words, the deformation becomes non-orientation preserving, and consequently the dynamics, not the choice of the coordinate system, makes the shear component non-zero. This is the physical meaning of the first term on the right-hand side of eqn. (12).

2.3 Field Theoretical Criteria of Plastic Deformation and Fracture

The explanations in the preceding section lead to the following criteria regarding the transitional stages from the elastic to plastic regime (Stage 1 criterion) and the plastic to fracturing regime (Stage 2 criterion).

2.3.1 Stage 1 Criterion

The first stage is that the displacement field starts to have rotational feature. This can be represented by

$$\nabla \times \vec{\omega} \neq 0 \tag{13}$$

on the right-hand side of eqn. (12). From the field theoretical viewpoint, this is the stage where the material cannot be represented by a single orientation-preserving mapping. Consequently, the displacement field becomes rotational. From the viewpoint of energy dissipation, the second term on the right-hand side of eqn. (12) represents momentum loss of the unit volume by means of material flow out. At this stage, it does not represent vigorous momentum loss. However, since the longitudinal effect does not exert elastic force, the displacement field stops showing longitudinal wave characteristics. Instead, the $\mu\nabla\times\vec{\omega}$ terms exert transverse (shear) recovery force, and consequently, the displacement field starts to shows transverse wave characteristics[16,17]. This transition can be observed as curved contours in the interferometric image patterns (fringe patterns).

2.3.2 Stage 2 Criterion

The second stage is characterized as the final stage of deformation where dynamics is dominated by the energy dissipation represented by $\mu\vec{j}$. At the same time, the effect of the first term representing the transverse wave characteristics vanishes. This causes the transverse displacement wave to decay. At the same time, since the $\mu\nabla\times\vec{\omega}$ term that causes the rotational feature of the displacement pattern vanishes, the displacement contours observed in the interferometric fringes patterns become straight.

More details about these criteria observed as the changes in the fringe patterns are discussed in the next section.

3. Experimental

A number of optical interferometric experiments have been carried out to study the field theoretical approach[10,17,19,20]. In particular, the stage 1 and stage 2 criteria have been experimentally investigated under various conditions. In this section, some of these experiments are discussed.

3.1 Electronic Speckle-Pattern Interferometry

Fig. 2 illustrates a typical arrangement of this type of experiment. The specimen is attached to a tensile machine, and pulled at a constant pulling rate. The interferometer is a typical dual-beam in-plane sensitive configuration, [11] consisting of a few mW-class helium-neon laser as the laser source, and optical systems comprised of a beam splitter, two folding mirrors and beam expanders. The

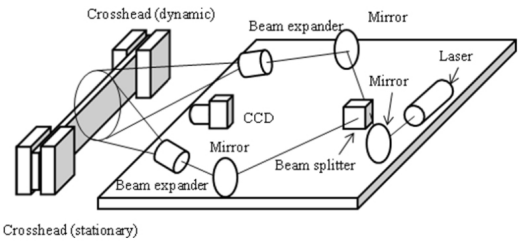

Fig. 2 Experimental arrangement with typical ESPI setup

CCD (charged couple device) camera takes images of the specimen at a constant frame rate as the tensile load is applied. The images taken by the CCD camera are transferred to computer memory where an image taken at each time step is subtracted from the image taken at a certain time steps before. In this fashion, the so-called subtraction fringe patterns such as the one shown in Fig. 3 are formed. Each dark stripe represents a contour of equi-displacement. When the interferometer is sensitive to horizontal displacement, as is the case of Fig. 2, the contours indicate horizontal displacement. Detailed information regarding ESPI can be found elsewhere[11].

3.2 Plastic Deformation and Fracture Criteria

Fig. 3 shows interferometric fringe patterns obtained in a tensile analysis on a tin specimen [10]. In this experiment, a vertically sensitive ESPI setup is arranged in addition to the horizontal setup so that horizontal and vertical displacement data can be taken simultaneously. The specimen is 100 mm long, 20 mm wide and 0.4 mm thick. One side of the specimen is curved as seen in Fig. 3 so that fracture is necessarily initiated on the known (curved) side. The horizontal width is narrowest (15 mm) at the vertical center. In Fig. 3, the images in the upper row are fringe patterns formed by the horizontally-sensitive ESPI setup (called the horizontally-sensitive fringe patterns) and those in the lower row are formed by the vertically-sensitive setup (vertically-sensitive fringe patterns). The plot in Fig. 4 is the loading characteristics recorded as the fringe patterns in Fig. 3 are formed. Labels (a) – (e) in Fig. 4 indicate the loading level at which the images in Fig. 3 of the same label are formed.

To examine the fringe patters from the viewpoint of the Stage 1 and Stage 2 criteria described in the preceding section, consider the physical meaning of the fringe patterns. Since the fringe patterns are formed by subtracting an image taken at a time from one taken at another time, the displacement contours are proportional to the displacement that each point of the material experiences between the two times. If the interferometer is sensitive to horizontal/vertical displacement, the dark fringes represent contours of constant horizontal/vertical component (defined as the x and y-component, respectively) of the displacement. Below we examine the expected fringe patterns for each criterion.

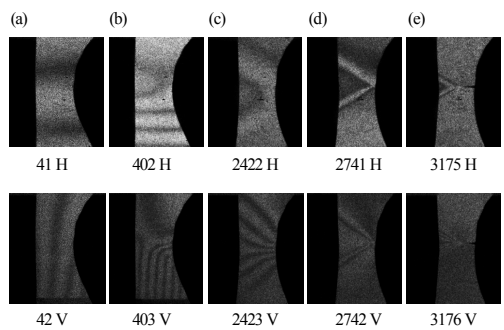

Fig. 3 Horizontally (upper) and vertically-sensitive (lower) fringe patterns

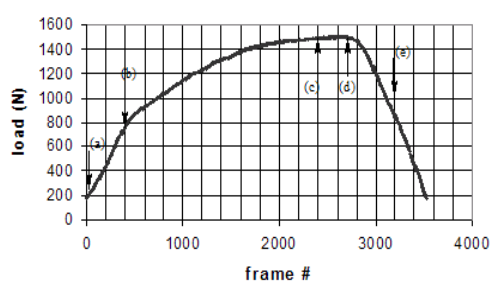

Fig. 4 Loading characteristics

3.2.1 Stage 1: Initiation of Plastic Deformation

Rewrite the condition $\nabla \times \vec{\omega} \neq 0$ in two-dimensions in terms of the x and y -components of the translational displacement (ξ_x and ξ_y).

$$(\nabla \times \vec{\omega})_x = \frac{\partial \omega_z}{\partial y} = -\frac{\partial^2 \xi_x}{\partial y^2} + \frac{\partial^2 \xi_y}{\partial x \partial y} \quad (14)$$

$$(\nabla \times \vec{\omega})_y = -\frac{\partial \omega_z}{\partial x} = \frac{\partial^2 \xi_x}{\partial x \partial y} - \frac{\partial^2 \xi_y}{\partial x^2} \quad (15)$$

A fringe pattern formed by a horizontally-sensitive interferometer indicates conditions (14) and (15) via the first terms on the right-hand side as the fringes represent contours of ξ_x. Similarly, a fringe pattern formed by a vertically-sensitive interferometer indicates them via the second terms. This means that in a horizontally-sensitive fringe pattern, $(\nabla \times \vec{\omega})_x \neq 0$ means the fringes have quadratic or higher dependence on y [the first term on the right-hand side of eqn. (14) is non-zero]. In other words, the fringes are at least horizontally parabolic. On the other hand, $(\nabla \times \vec{\omega})_y \neq 0$ means the fringes have both x and $y-$ dependences, or at least they are tilted on the $x-y$ plane. The features observed in a vertically-sensitive fringe pattern can be argued in the same fashion. Table 1 summarizes these features where “H/V-parabola“ and “tilted“ denote these features.

3.2.2 Stage 2: Initiation of Fracture

In Stage 2, the shear force becomes inactive making $\nabla \times \vec{\omega} = 0$. In this situation, the only mechanism to change the acceleration of the unit volume [the left-hand side of eqn. (12)] is the momentum loss represented by eqn. (11). The fringe patterns are characterized by the following features. In a horizontally-sensitive fringe pattern, $(\nabla \times \vec{\omega})_x = 0$ makes $\partial^2 \xi_x / \partial y^2 = 0$ or the corresponding fringe a straight line. $(\nabla \times \vec{\omega})_y = 0$ makes $\partial^2 \xi_y / \partial x \partial y = 0$ or the corresponding fringe becomes a straight line parallel to either the x or y axis. The features observed in a vertically-sensitive fringe pattern can be argued in the same way, as shown in Table 2. Here // to x/y denotes that straight fringes parallel to the x or y axis.

Table 1 Stage 1 conditions observed in fringe patterns

Interferometer’s sensitivity	$(\nabla \times \vec{\omega})_x \neq 0$	$(\nabla \times \vec{\omega})_y \neq 0$
Horizontal	H-parabola	tilted
Vertical	tilted	V-parabola

Table 2 Stage 2 conditions observed in fringe patterns

Interferometer sensitivity	$(\nabla \times \vec{\omega})_x = 0$	$(\nabla \times \vec{\omega})_y = 0$
Horizontal	Linear	// to *x*/*y*
Vertical	// to *x*/*y*	linear

Now observe fringe patterns in Fig. 3 from this viewpoint. At time (a), both the horizontally- and vertically-sensitive fringe patterns show straight fringes, indicating that at this stage deformation is still elastic (Stage 1 condition has not been satisfied) and therefore, $(\nabla \times \vec{\omega})_x = 0$. At times (b) and (c), the horizontally-sensitive fringes show a horizontal parabola near the middle and straight lines toward the lower end. This indicates that near the middle of the specimen the deformation is plastic whereas towards the end where the width is greater the deformation is still elastic. The vertical fringe pattern shows the corresponding feature. Loading characteristics in Fig. 4 indicates that at times (b) and (c) the deformation is apparently in the plastic regime.

At time (d), the horizontal fringe pattern clearly shows the feature identified as $(\nabla\times\vec{\omega})_x=0$ while the feature representing $(\nabla\times\vec{\omega})_y=0$ is not observed. The loading curve at this time is near the ultimate strength. These altogether can be interpreted as at this stage the material still exerts the vertical force but not horizontal force. The vertically-sensitive fringe pattern show features consistent with the horizontally-sensitive fringe pattern. Very interestingly, this straight-line pattern sweeps across the width of the specimen from the right to left. This can be interpreted as the specimen meets the Stage 2 criterion from the right side.

3.3 Residual Stress Analysis

In the next series of experiments[20], the same idea is applied to analysis of load hysteresis. The specimen (0.5 mm-thick pure aluminum sheet cut into 4 mm in gauge width and 25 mm in gauge length, and subsequently annealed at 400 °C for 30 min.) is initially tensile loaded to a certain stress level (preloaded), and after removal of the preload, it is reloaded to various stress levels. Then the fringe patterns resulting from the reloading are examined regarding whether or not the effect of the initial load is revealed as any specific features in the shape of the fringes. Fig. 5 shows three load levels at which the analyses are made. The interferometer used in this analysis is sensitive to horizontal displacement, whereas the tensile direction is also horizontal.

In the first experiment, the specimen is loaded till fracture for the purpose of obtaining the baseline data. Fig. 6 shows the fringe patterns observed in this experiment at the stress level indicated at the top left corner of each image.

In the second experiment, the specimen is preloaded to 30 MPa (point A in Fig. 5), and reloaded to the same stress level of 30 MPa after released from the preload. Fig. 7 compares

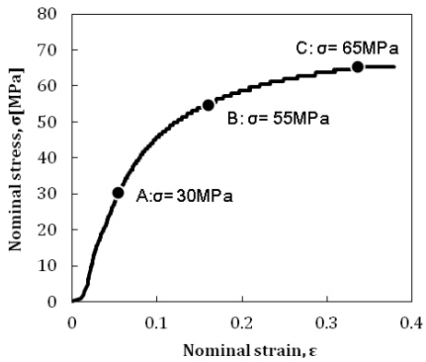

Fig. 5 Loading curve of the initial (preload) pull

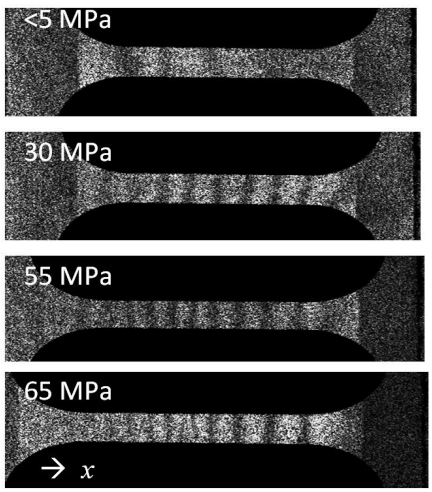

Fig. 6 Fringe patterns observed in the preload

the fringe patterns observed at 30 MPa in the preload (upper) and in the reload (lower). These fringe patterns show clear distinctions. In the initial pull (preload), the fringes are mostly vertical, slightly inclined clockwise, whereas some (e.g., the rightmost fringe) show the parabolic nature discussed above (see text near Table 1). The fringes observed at 30 MPa on the second pull (reload), on the other hand, are wavy and mostly horizontal. The wavy part clearly shows the parabolic nature. In accordance with Table 1 under the row labeled "Horizontal", the pattern observed in the reload indicates that the specimen exerts resisting force proportional to $(\nabla\times\vec{\omega})$ both in the horizontal and vertical directions. The observed difference between the preload and reload can be

qualitatively explained as follows. When the specimen is loaded to 30 MPa in the initial pull, the material already experiences partial plastic deformation. Both the first term representing recovery force and the second term representing the energy-dissipative plastic effect are active on the right-hand side of eqn. (12). However, at this stage, the overall deformation is dominantly elastic. Consequently, the fringes are mostly vertical and straight. The plastic effect is observed in that the fringes are tilted ($\omega_z \neq 0$) and some are somewhat parabolic ($(\nabla \times \vec{\omega})_z \neq 0$). The tilting effect is caused by the fact that the material experiences greater stretch towards the bottom side of the specimen than the top side (that is why the fringes are denser near the bottom than the top of the specimen). This excess stretch (lateral differential displacement) is due to permanent deformation (i.e., the material experiences partial yield near the bottom side). Since this phenomenon takes place gradually, the fringe tilt observed at each time step of fringe pattern formation is small.

When the specimen is released from the preload, the deformation is recovered as much as the recoverable portion associated with the recovery force represented by the first term on the right-hand side of eqn. (12). The excess stretch discussed in the preceding paragraph is not recovered. Therefore, when the specimen is reloaded to the same stress level as the preload, only the recoverable portion of displacement is observed. Being proportional to $\nabla \times \vec{\omega}$, the corresponding fringes are wavy (vortex-like).

It is interesting to note that the curvatures of the parabolic fringe pattern observed in Figs. 3 and 6 are substantially different (both are observed in the initial pull). Based on the same idea as the above-mentioned excess stretch near one side of the specimen, it is natural to assume that the greater the degree of differential displacement, the steeper the parabolic curvature.

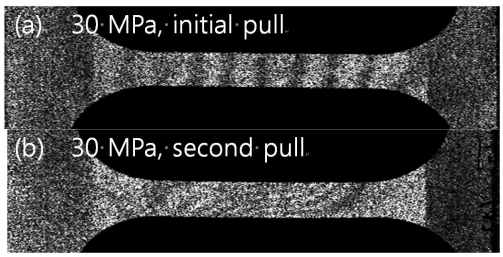

Fig. 7 Reload experiment on aluminum specimen. (a): initial pull at 30 MPa, (b) second pull at 30 MPa (preload at 30 MPa)

From this viewpoint, it is reasonable to say that the specimen in Fig. 3, which has horizontal asymmetry in such a way that the curved side is weaker than the straight side, experiences greater differential displacement than the case where both sides are straight, and therefore shows a steeper curvature in the parabolic fringe pattern.

In the third experiment, the specimen is preloaded to 55 MPa in the initial pull, and the fringe patterns are examined at 25 MPa (lower than the preload level) and 65 MPa (higher than the preload) in the second pull.

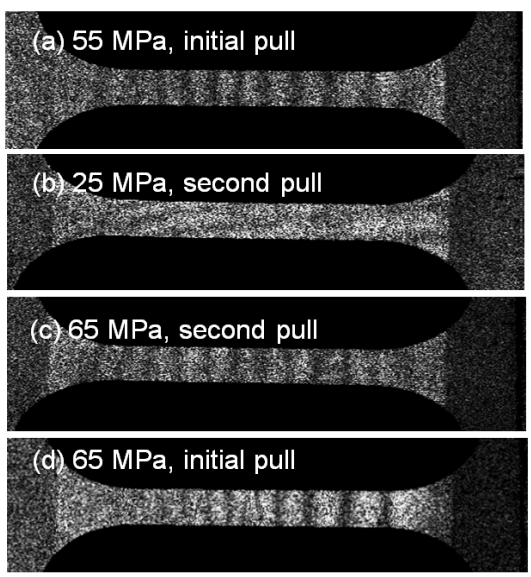

Fig. 8 Reload experiment on aluminum specimen up to 55 MPa. (a): initial pull 55 MPa, (b): reload at 25 MPa after preloaded to 55 MPa, and (c) reload at 65 MPa after preloaded to 55 MPa, (d) initial pull at 65 MPa

4. Conclusions

The gist of the field theoretical approach has been presented. The Stage 1 and Stage 2 criteria of plastic deformation derived by the field theoretical approach have been applied to diagnosis of deformational status of metal specimens. The features observed in the interferometric fringe patterns are consistent with the criteria. The hysteresis of loading on aluminum specimens have been revealed by this technique. Other applications to nondestructive evaluation of metal objects are expected. As to field applications of load hysteresis analysis, this technology in the current form has limitations; it requires an external load to form fringe patterns to be examined. In many occasions, application of external loads to the object under inspection is difficult. Further investigation to improve this aspect is necessary.

Acknowledgment

The author is grateful to various supports provided by Southeastern Louisiana University. Helpful discussion by Cesar Sciammarella of Illinois Institute of Technology is highly appreciated.

References

[1] J. M. Barsom and S. at. Rolfe, "Fracture and fatigue control in structures," ASTM Philadelphia, (1999)

[2] S. Yoshida, "Dynamics of plastic deformation based on restoring and energy dissipative mechanisms in plasticity," *Physical Mesomech.*, Vol. 11, Iss. 3-4, pp. 137-143 (2008)

[3] S. Yoshida, "Physical meaning of physical-mesomechanical formulation of deformation and fracture," *AIP Conference Proceedings*, Vol. 1301, pp. 146-155 (2010)

[4] S. Yoshida, "Scale-independent approach to deformation and fracture of solid-state materials," *J. Strain Analysis*, Vol. 46, No. 5, pp. 380-388 (2011)

[5] V. E. Panin, Yu. V. Grinaev, V. E. Egorushkin, I. L. Buchbinder and S. N. Kul'kov, "Spectrum of excited states and the rotational mechanical field," *Sov. Phys. J.*, Vol. 30, pp. 24-38 (1987)

[6] V. E. Panin (Ed.), "Physical Mesomechanics of Heterogeneous Media and Computer-Aided Design of Materials," Vol. 1, Cambridge International Science, Cambridge (1998)

[7] I. J. R. Aitchson and A. J. G. Hey, "Gauge Theories in Particle Physics," IOP Publishing, Bristol and Philadelphia (1989)

[8] L. D. Landau and E. M. Lifshitz, "Theory of Elasticity, 3rd Ed.," *Course of Theoretical Physics*, Vol. 7, Butterworth-Heinmann, Oxford (1986)

[9] S. Yoshida, "Consideration on fracture of solid-state materials," *Phys. Lett. A*, Vol. 270, Iss. 6, pp. 320-325 (2000)

[10] S. Yoshida, R. L., Rourks, T. Mita and K. Ichinose, "Physical mesomechanical criteria of plastic deformation and fracture," *Phys. Mesomech*. Vol. 12, Iss. 5-6, pp. 249-253 (2009)

[11] R. S. Sirohi (Ed.), "Speckle Metrology," Marcel Dekker, Inc., New York (1993)

[12] J. E. Marsden and T. J. R. Hughes, "Mathematical Foundations of Elasticity," Prentice-Hall, Englewood Cliffs (1983)

[13] E. H. Dill, "Continuum Mechanics," Taylor & Francis, Inc., New York (2006)

[14] I. R. Kenyon, "General Relativity," Oxford Univ. Press., Oxford (1996)

[15] S. Yoshida, "Scale independent approach to deformation and fracture," Proc. 2012 Soc. Exp. Mech. 2012 Annual Meeting (in press)

[16] S. Yoshida, "Interpretation of meso-mechanical behaviors of plastic deformation based on analogy to Maxwell electromagnetic theory," *J. Phys. Meso. Mech.* Vol. 4, Iss. 3, pp. 29-34 (2001)

[17] S. Yoshida, B. Siahaan, M. H. Pardede, N. Sijabat, H. Simangunsong, T. Simbolon and A. Kusnowo, "Observation of plastic deformation wave in a tensile-loaded aluminum-alloy," *Phys. Lett. A,* Vol. 251, Iss. 1,4, pp. 54-60 (1999)

[18] S. Yoshida, "Optical interferometric study on deformation and fracture based on physical mesomechanics," *J. Phys. Mesomech.*, Vol. 2, Iss. 4, pp. 5-12 (1999)

[19] S. Yoshida, G. A. Gaffney and K. Yoshida, "Revealing load hysteresis based on physical-mesomechanical deformation and fracture criteria," *Phys. Mesomech.*, Vol. 13, Iss. 5-6, pp. 337-343 (2010)

[20] T. Sasaki and S. Yoshida. "Revealing load hysteresis based on electronic speckle pattern interferometry and physical mesomechanics," *Phys. Mesomech.*, April 2012 issue (in press)